Journal of Vacuum Science and Technology A

RESEARCH ARTICLE | JULY 09 2013

Tin oxide atomic layer deposition from tetrakis(dimethylamino)tin and water

Marja N. Mullings; Carl Hägglund; Stacey F. Bent

J. Vac. Sci. Technol. A 31, 061503 (2013)
https://doi.org/10.1116/1.4812717

Tin oxide atomic layer deposition from tetrakis(dimethylamino)tin and water

Marja N. Mullings, Carl Hägglund, and Stacey F. Bent[a)]
Department of Chemical Engineering, Stanford University, Stanford, California 94305

(Received 23 March 2013; accepted 18 June 2013; published 9 July 2013)

Due to the abundance and usefulness of tin oxide for applications such as transparent conductors, sensors, and catalysts, it is desirable to establish high quality atomic layer deposition (ALD) of this material. ALD allows for uniform, conformal coating of complex topographies with ultrathin films and can broaden the applicability of tin oxide to systems such as nanostructured solar cells. The present work examines the ALD of tin oxide by means of the precursor tetrakis(dimethylamino)tin and water as a counter-reactant. Low temperature growth in the range of 30–200 °C on Si(100) and glass substrates is studied. It is found that the growth rate increases with reduced temperature, up to ~2.0 Å/cycle at 30 °C, as compared to 0.70 Å/cycle at 150 °C. The ALD process is established to be saturated even at the lowest temperature studied, for which the film contamination levels are below the detection limits of x-ray photoelectron spectroscopy. As-deposited films are smooth (rms roughness of 33 Å for a 460 Å thick film deposited on Si at 150 °C) and amorphous according to x-ray diffractometry. However, post-annealing to 600 °C in nitrogen leads to the formation of polycrystalline rutile SnO_2. The optical constants obtained from variable angle spectroscopic ellipsometry suggest that as-deposited films have amorphous type bandgaps, which decrease with increasing temperature and film thickness. High quality, amorphous SnO_2 films with moderately tunable optical properties are thus obtained by ALD at temperatures as low as 30 °C using a commercially available tin precursor and water. © *2013 American Vacuum Society*.
[http://dx.doi.org/10.1116/1.4812717]

I. INTRODUCTION

Tin oxide, SnO_x, $1 \leq x \leq 2$, is a wide bandgap semiconductor material with excellent optical, electrical, and chemical properties.[1–5] As a consequence, SnO_x is used in a variety of applications including gas sensing,[6–9] surface coatings for functional glasses,[10–12] field effect transistors,[13,14] catalysis,[15–17] and as transparent conducting oxides (TCOs) in photovoltaics and displays.[18–22] As part of the solid solution of indium tin oxide, it produces one of the most commercially important TCOs.[23] In parallel with its large number of applications, many deposition techniques exist for thin films of SnO_x including chemical vapor deposition (CVD),[24–28] spray-pyrolysis,[29,30] sputtering,[31] and atomic layer deposition (ALD).[28,32–44] ALD is the focus of this study because it has the potential to enhance the ways SnO_x may be integrated with other materials and to broaden its applications.

For the purpose of growing uniform and conformal thin films, ALD is an increasingly popular method.[45–49] This vacuum deposition technique is based on alternating gas-surface reactions separated by inert purges allowing for self-limited growth, ideally yielding uniform and conformal films independent of substrate geometry. ALD has been used to deposit a wide range of materials, including metals,[33,47,50–54] metal oxides,[47,53,55–57] and metal sulfides.[58–61] It has also allowed for the area-selective growth of a variety of materials.[45–49,62–69] Moreover, conformal coverage of three-dimensional substrates is a characteristic feature resulting from the self-limited growth mechanism of ALD.[9,54,70–74]

Starting in the 1990s, ALD was explored as a way to deposit SnO_x films.[37,42,43] As with many other ALD systems, the choice of precursors for depositing SnO_x was derived from related CVD processes.[42,43] Depending on growth temperature, some of these films had the advantage of being crystalline as deposited, but yielded corrosive and equipment-damaging byproducts due to the use of halogenated precursors.[33,36,42] Elam and coworkers were the first to publish on the development of a SnO_2 ALD process that used nonhalogenated precursors[35] with further developments by Heo and coworkers.[32,38] The former work elucidated the ALD process using tetrakis(dimethylamino)tin (TDMASn) and H_2O_2 and determined an average growth rate of 1.2 Å/cycle, a temperature window of 50–200 °C and an average 94% transmission of visible light for a film thickness of 140 nm. Growth rates of SnO_2 using TDMASn and other oxidant counter-reactants of ozone and water were also reported, although these particular ALD processes and the resultant films were not described in detail.

In this work, we build upon these previous results and further elucidate the ALD of SnO_x films using the same nonhalogenated precursor, TDMASn, with water as the counter-reactant. We demonstrate the ability to deposit SnO_x at temperatures as low as 30 °C, at growth rates equaling or exceeding that of ALD with H_2O_2 as the counter-reactant. Compared to harsher counter-reactants such as H_2O_2 and O_3, water can make SnO_x ALD more compatible with sensitive applications in, for instance, biological and polymeric systems. The use of water may further reduce operating costs and ease integration into existing processes. Moreover, water is the counter-reactant of the well-studied ZnO ALD system based on diethyl zinc.[75,76] SnO_x ALD with water is therefore

[a)]Electronic mail: sbent@stanford.edu

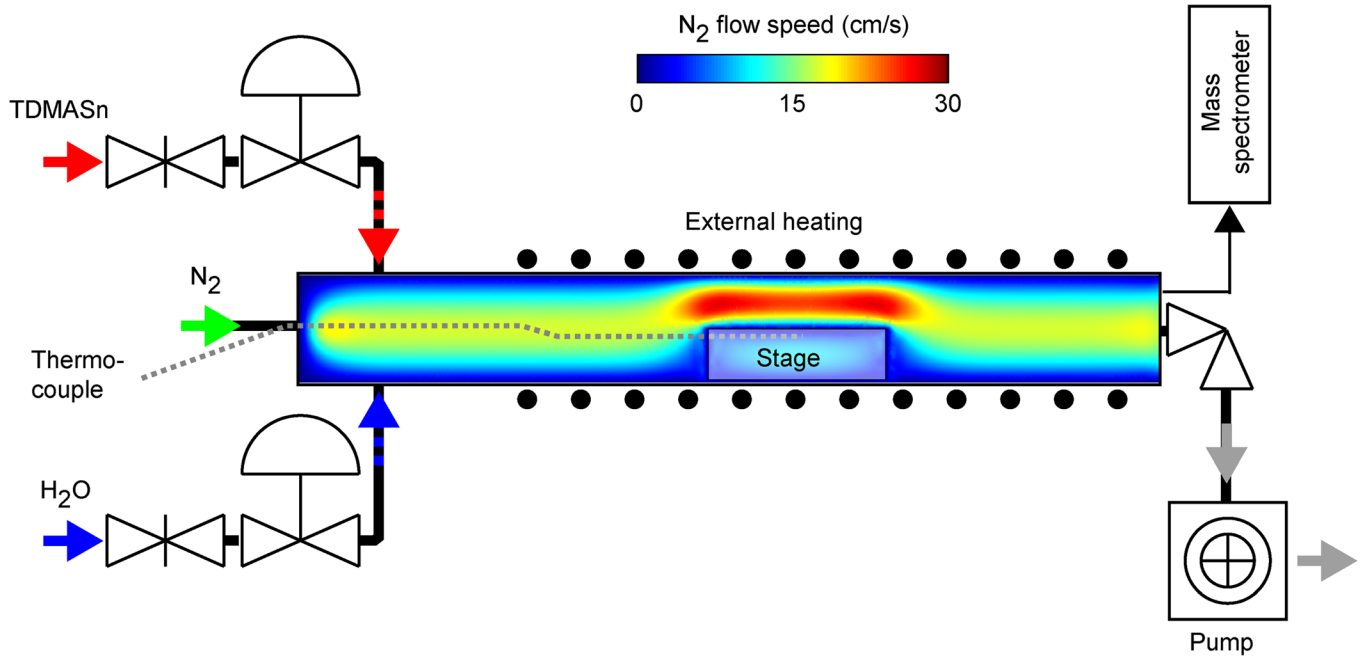

FIG. 1. (Color online) Schematic of the custom-built, hot-wall ALD reactor. The main part is a cylindrical tube, heated externally. The tube is fitted with inlets for N_2 carrier gas and precursors close to its upstream end. A sample stage with *in-situ* temperature monitoring is positioned near the center of the tube. A separately pumped mass spectrometer is used to analyze gas sampled downstream of the stage by means of a needle valve. The calculated carrier gas flow and diffusion through the tube indicate even distribution of the gas. The flow profile in the mid section of the tube is shown.

of potential interest for the development of a thermal zinc tin oxide (ZTO) ALD process, and as such provides an opportunity for ALD of ZTO with regard to its role as a transparent conducting oxide.[77]

II. EXPERIMENTAL DETAILS

The ALD experiments were carried out in a custom-built, viscous-flow, hot-wall reactor shown schematically in Fig. 1. The substrate was loaded into a tube style body (with 35 mm diameter and ~300 mm length) on a stage with temperature monitoring through an incorporated thermocouple placed close to the substrate position. Nitrogen carrier gas (99.999%, Air Products) at 10 sccm was flowed through the tube, enabling efficient transport of the precursors introduced at its upstream end. The reactor was evacuated by a rotary vane pump (Alcatel), resulting in a typical pressure of 100 mTorr during ALD. Precursor pressure pulse amplitudes were in the range of 1–50 mTorr. Numerical calculations using the finite element method based on software from COMSOL Multiphysics were used to ensure adequate reactor design through modeling of carrier gas flow and diffusion as described elsewhere.[78] A quadrupole mass spectrometer (SRS RGA200) was used to sample the gas composition through a needle valve downstream of the ALD substrate.

TDMASn (Strem, >99% purity) was used as a precursor with deionized water as the counter-reactant. The TDMASn precursor vial was heated to 45 °C and the line used to transport it into the reactor was heated to similar or higher temperature to ensure consistent vapor injections for deposition. Due to dilution in the carrier gas and effective pumping of the reactor, precursor condensation on the substrate was avoided even when the substrate temperature was slightly below the precursor vial temperature.

Substrates for SnO_x ALD included n-type Si(100) with phosphorous dopant and a resistivity of 1.0–5.0 Ω-cm (WRS Materials) and microscope slide glass (Thermo Scientific, Gold Seal, CAT. NO. 2050). All substrates were precleaned using a Piranha etch (70% H_2SO_4 and 30% H_2O_2) to remove organics and generate a chemical oxide. SnO_x thin films were deposited directly onto this chemical oxide. After loading into the reactor, samples were allowed to outgas for at least 20 min before the reactor was heated to achieve the desired substrate temperature. After injection of a given precursor for a certain pulse time, the excess precursor was purged with nitrogen before the counter-reactant was introduced. The ALD sequence is compactly expressed as t_1:t_2:t_3:t_4, where t_1 and t_3 correspond to the pulse lengths of TDMASn and water, respectively, and t_2 and t_4 to N_2 purge times following these doses. A typical timing sequence was 1:30:2:30 s.

The deposited SnO_x films were analyzed *ex-situ* by a variety of methods. A PHI VersaProbe 5000 scanning X-ray photoelectron spectrometer with Al Kα radiation was used to determine elemental compositions, using the C1s peak at 285.0 eV as a reference. After initial survey scans, adventitious carbon was removed by Ar^+ sputtering for 12 s (1 keV, 0.5 μA, 1 mm × 1 mm at 45° incidence from the sample). As-deposited films were annealed under flow of N_2 (1 cm^3/s) in a Mellen Series SC13R-1300 °C, single zone, split hinged, round tubular furnace with an Omega 7832 process controller at 500 °C and 600 °C. X-ray diffraction (XRD) measurements were taken as a function of anneal temperature using the

PANalytical X'Pert PRO system in parallel beam mode with Cu Kα radiation at 45 kV and 40 mA. Film thickness and optical constants of SnO_x deposited on Si(100) were determined using a J.A. Woollam M2000 variable angle spectroscopy ellipsometer (VASE). Plan view and cross-sectional images of SnO_x film morphology were examined using a FEI Magellan 400 XHR scanning electron microscope (SEM) with a field emission gun source (5 kV and 25 pA). Optical extinction spectra of films deposited on microscope slide glass were recorded using a Varian Cary 6000i UV-Vis-NIR spectrometer. Topographical information for the films was determined by atomic force microscopy using a Park System atomic force microscope (AFM) in tapping mode.

III. RESULTS AND DISCUSSION

A. ALD growth characterization

Considering the surface reactions involved in the process is important for understanding the film growth by ALD. A possible mechanism for the SnO_2 ALD using TDMASn and H_2O_2 based on *in-situ* quartz crystal microbalance analysis was previously suggested.[35] The corresponding reaction mechanism with water as the counter-reactant is

$$(OH)_x^* + Sn(DMA)_4 \rightarrow (O)_xSn(DMA)_{4-x}^* + xHDMA \quad (1)$$

$$(O)_xSn(DMA)_{4-x}^* + 2H_2O \rightarrow (OH)_x^* + SnO_2 + (4-x)HDMA, \quad (2)$$

where DMA represents the dimethylamino ligand, HDMA is dimethylamine (released to gas phase), the * refers to surface-bound species, and x is the number of DMA ligands released during the TDMASn pulse. Measurements indicated that $x \approx 2.5$ with H_2O as the counter-reactant, compared to a higher value of $x \approx 3$ when using H_2O_2. They suggest that this reaction stoichiometry is consistent with the lower growth rate observed with H_2O at higher temperatures and largely reflects a lower degree of surface hydroxylation.[35] Reaction (1) shows the importance of the surface hydroxylation state for the initial adsorption of the precursor.

To determine the conditions for saturated ALD of SnO_x in our studies, the growth rate as a function of TDMASn precursor pulse time (t_1) was investigated. Thin films of SnO_x were deposited on Si(100) at 150 °C for 200 cycles with a timing sequence of t_1:30:2:30 s. The purge times of 30 s were conservatively selected to be long enough to purge away excess reactant, as judged by the downstream gas composition monitored by mass spectroscopy. In this way, contributions from CVD were minimized. Average film thicknesses determined by VASE were used to calculate the SnO_x growth rate. Figure 2(a) represents the saturation curve for TDMASn and shows that, within the uncertainty of the experiment, saturated behavior is reached already for the shortest pulse time of 0.5 s at 150 °C. The TDMASn pulse time was fixed to 1 s to ensure saturation in subsequent experiments. The SnO_x growth as a function of water pulse length (t_3) was also investigated following a similar procedure as before but using a pulse-purge sequence of 1:30:t_3:30 s. Figure 2(b) shows that a relatively steady growth rate is established after 0.5 s H_2O pulse times. These precursor saturation studies suggest that saturated growth is accomplished for a broad range of pulse lengths. We obtained growth rates with good reproducibility for a timing sequence of 1:30:2:30 s at 150 °C.

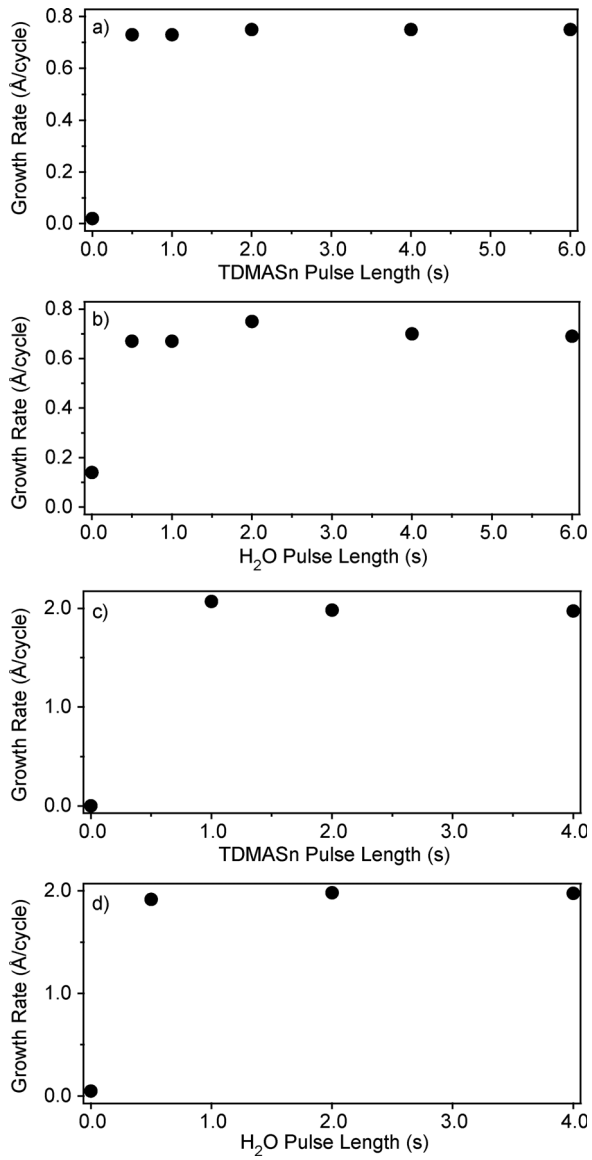

FIG. 2. SnO_x growth rate determined by VASE, as a function of (a) and (c) TDMASn pulse length t_1 for timing sequences of t_1:30:2:30 s and (b) and (d) H_2O pulse length t_3 for timing sequences of 1:30:t_3:30 s. The substrate was Si(100) at 150 °C for (a) and (b) and at 30 °C for (c) and (d).

The precise conditions for establishing ALD saturation in terms of precursor exposure time depend on the particular reactor design in addition to the choice of precursor and counter-reactant. The work of Elam and coworkers using the tin precursor, TDMASn, and H_2O_2 to deposit SnO_x by ALD showed a gradual approach toward saturated growth. To explain this gradual ascent toward saturation, it was proposed that DMA binds strongly to the hydroxylated substrate resulting in slow desorption, thereby limiting the adsorption of further TDMASn for pulse times below 2 s. However, this

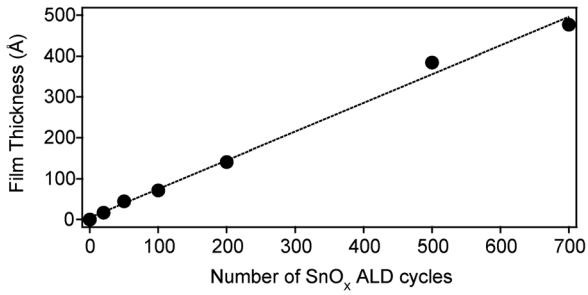

FIG. 3. SnO_x film thickness as a function of number of ALD cycles yielding a growth rate of 0.70 Å/cycle. Thicknesses were obtained using VASE for films deposited on Si(100) at 150 °C with a time sequence of 1:30:2:30.

effect was not observed in our studies in which water was used as the counter-reactant; for the pulse time intervals explored, there is little difference between growth rates at shorter (0.5 s) and longer pulse times (>1.0 s) suggesting that surface saturation occurred quickly.

Figure 3 presents the SnO_x film thickness as a function of number of ALD cycles over the range of 20 to 700 cycles. The data were collected using VASE for deposition on a Si(100) substrate at 150 °C with a timing sequence of 1:30:2:30 s. The linear dependence of film thickness on cycle number indicates sustained layer-by-layer growth characteristic of ALD. The average growth rate is 0.70 Å/cycle, in close agreement with the previously reported value at this temperature.[35]

Figure 4 shows the growth rate of SnO_x as a function of deposition temperature ranging from 30 to 200 °C. The growth rate displays a clearly decreasing trend with increasing deposition temperature over the entire interval, with a slight plateau in the range from 150 to 175 °C. The growth rate at 30 °C of ~2.1 Å/cycle is about four times higher than that at 200 °C where it is ~0.5 Å/cycle. This sensitivity to deposition temperature is much higher than that reported for the TDMASn and H_2O_2 ALD system.[35] In that system, the growth rate varied only from ~1.6 Å/cycle at 50 °C to ~1.3 Å/cycle at 200 °C, respectively. Also, a region of near constant growth rate was shown between 100 and 200 °C. On the other hand, it is interesting to note that the use of water as a counter-reactant results in a higher growth rate at low temperatures than that previously observed with H_2O_2. Comparing with the data presented by Elam and coworkers, the crossover is around 80 °C. So even though the use of

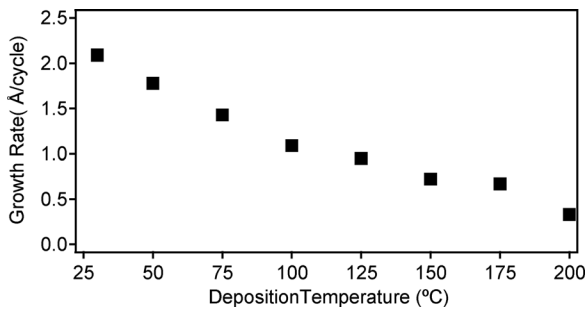

FIG. 4. SnO_x ALD growth rate as a function of temperature determined using VASE for films deposited on Si(100) for 200 cycles with timing sequence 1:30:2:30 s.

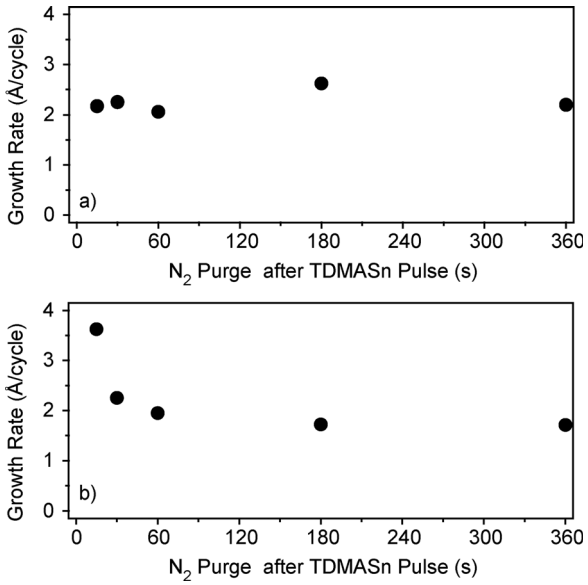

FIG. 5. SnO_x growth rate at 30 °C determined by VASE as a function of nitrogen purge time following (a) TDMASn pulse length and (b) H_2O pulse length for timing sequences of $1:t_2:2:t_4$ s. The substrate was Si(100).

water as a TDMASn counter-reactant is expected to result in lower concentration of reactive surface hydroxyl groups at the higher temperatures investigated, the overall SnO_x growth rate is higher at the lower temperatures.

Larger coverages of more loosely bound molecular water or water-derived species may be available in this temperature range and capable of contributing to the growth observed. However, measurement of the growth rates at 30 °C presented in Figs. 2(c) and 2(d) shows that the reactions still saturate with the water precursor pulse length. Furthermore, at this low temperature, growth rate purge time dependence following the 1s TDMASn pulse [Fig. 5(a)] and 2 s water pulse [Fig. 5(b)] shows saturated growth characteristic of ALD. Taken together, these data imply that the water and water-derived species present at the surface contribute to the growth of the SnO_x film at this low temperature. Though *in-situ* or theoretical studies may be needed to elucidate the detailed nature of the water derived species responsible for the high growth rate in this regime, it is a significant finding that growth saturation behavior, characteristic of ALD, can be achieved at 30 °C.

B. Film characterization and properties

X-ray photoelectron spectroscopy (XPS) was performed to determine the film composition. Figure 6 shows an XPS survey scan of a 46 nm SnO_x film deposited at 150 °C on Si(100) after removal of adventitious surface carbon by Ar^+ sputtering. The data show the presence of both Sn and O, confirming the deposition of an oxide of tin; no carbon or nitrogen contamination is observed.

Providing a quantitative stoichiometry of the SnO_x film from XPS data is difficult. The atomic ratio of Sn:O before sputtering was close to 1:2, which would suggest a stoichiometry of SnO_2. After sputtering the ratio of Sn:O was closer

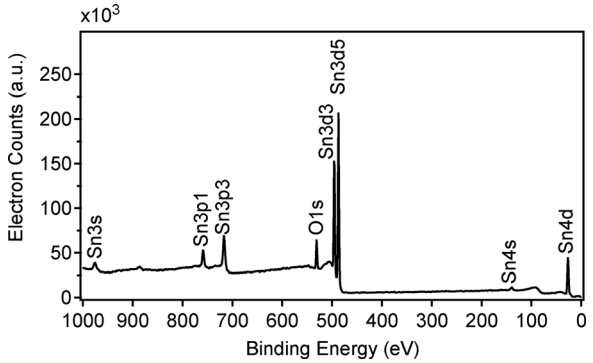

FIG. 6. X-ray photoelectron spectroscopy survey scan of 46 nm SnO_x film deposited on Si(100) at 150 °C after Ar^+ sputtering.

to 1:1 suggesting a stoichiometry of SnO. However, the possibility of preferential sputtering of one element over another leads to uncertainty in the compound stoichiometry. Using the core level shifts to determine the oxidation state of as-deposited SnO_x using XPS is also challenging due to the closeness in values of the $Sn3d_{5/2}$ binding energies for SnO (486.8 eV) and SnO_2 (487.2 eV).

XPS spectra were also obtained for SnO_x films as a function of ALD temperature. The data show that nearly carbon-free films can be deposited at all growth temperatures studied. Carbon levels determined by XPS as a function of deposition temperature are shown in Supporting Information,[79] Fig. S1, both before and after Ar^+ sputtering to remove adventitious carbon. Although carbon is observed in all films before sputtering, the films were solely comprised of Sn and O after sputtering, independent of deposition temperature. Importantly, these data indicate that SnO_x ALD films can be deposited without significant carbon contamination even near room temperature. In contrast, nitrogen and carbon contamination was observed by Elam and coworkers when using H_2O_2 rather than H_2O at temperatures below ~100 °C.

The SnO_x films were examined by XRD both as deposited and after annealing in nitrogen. Figure 7 shows the XRD patterns as deposited and after nitrogen annealing to 600 °C; reference diffraction patterns of SnO and SnO_2 are included for comparison. For the as-deposited film at 150 °C, the film appears to be amorphous. Patterns appear but exhibit broad peaks upon annealing at 600 °C.

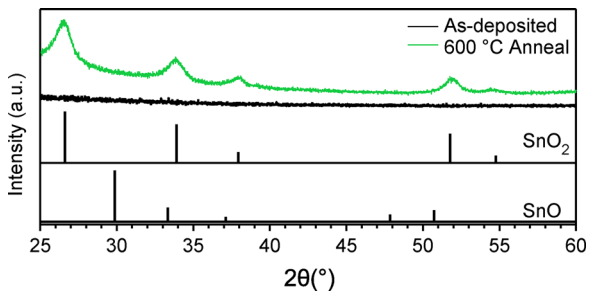

FIG. 7. (Color online) XRD patterns for a 130 nm film of SnO_x deposited on Si(100) at 150 °C as function of annealing temperature under flow of N_2, as-deposited (featureless black curve) and after 600 °C anneal (upper curve, with diffraction peaks).

The diffraction pattern after annealing is characteristic of the SnO_2 phase, including reflection of the (110), (101), (200), and (211) planes at 26.6°, 33.9°, 37.9°, and 51.8°. The diffraction peaks in Fig. 7 are indexed on the basis of the rutile SnO_2 unit cell. Patterns indicative of SnO for reflection of the (101) and (110) planes at 29.9° and 33.3° were not evident. The large width and low intensities of the peaks may be the result of small crystallites from incomplete crystallization as well as the relatively low thickness of the films (130 nm). The data strongly suggest that these films consist of rutile SnO_2.

The film morphology as a function of annealing temperature in N_2 is shown in Fig. 8 for a 46 nm thick SnO_x sample deposited at 150 °C on Si(100). Figure 8(a) indicates that the as-deposited film morphology is relatively smooth with little variation in features. From AFM (data not shown), the root mean squared (rms) roughness of the as-deposited film was 3.3 nm. Figures 8(b) and 8(c) show plan view SEM images of films annealed at 500 and 600 °C, respectively. Upon annealing, the film roughness increases and the crystallite size increases. The appearance of a more crystalline film is consistent with the diffraction pattern from XRD. The cross-sectional image in Fig. 8(d) of the film annealed at 600 °C provides more support for polycrystallinity. The rms roughness of this film was 4.5 nm as determined by AFM, which is larger than for the as-deposited case and consistent with the growth of larger crystallites.

The optical properties of the SnO_x films were analyzed using variable angle spectroscopic ellipsometry. The ellipsometry data were analyzed using a generalized oscillator model for the SnO_x layer. This model included a polynomial spline function (the psemi-m0 oscillator[80]) and pole terms in the infrared and ultraviolet, outside the measured range. The resulting optical constants are consistent with the Kramers–Kronig relation by construction.

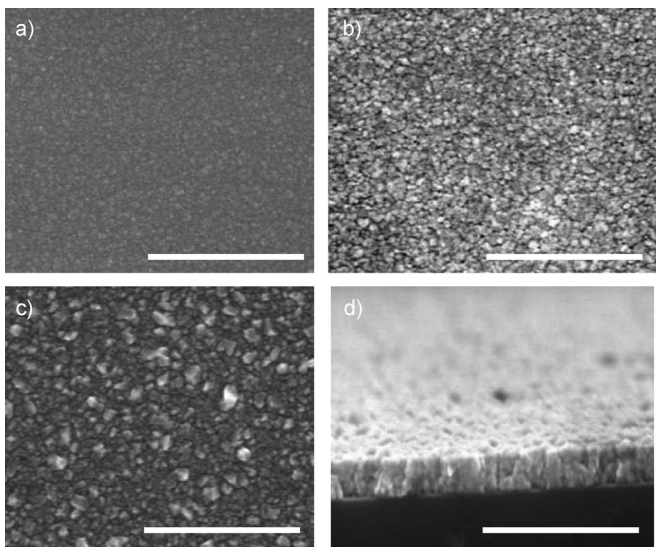

FIG. 8. SEM images of a 46 nm SnO_x film deposited on Si(100) at 150 °C (a) as-deposited; (b) post-500 °C anneal; (c) post-600 °C anneal; (d) cross-section of film post-600 °C anneal. The scale bars are 300 nm.

The resulting refractive index n and extinction coefficient k are displayed in Figs. 9(a) and 9(b) , respectively, for films deposited on Si(100) using a fixed number of 200 ALD cycles and varying substrate temperatures (30–200 °C). Both optical constants vary with temperature and display maximum values for films deposited around 150 °C. In the literature, (poly-) crystalline SnO_2 is typically ascribed a direct bandgap in the range of 3.6–4.0 eV.[4,81,82] In order to analyze the optical bandgaps of the SnO_x films produced here, their absorption coefficients were determined from $\alpha = 4\pi k/\lambda$, where λ is the wavelength of light. However, a direct bandgap dependence was not clear in a plot of $(\alpha\, h\nu)^2$ versus photon energy ($h\nu$). Rather, and more characteristic for amorphous and indirect bandgap semiconductors,[83] a plot of the function $(\alpha\, h\nu)^{1/2}$ versus photon energy revealed a linear segment close to the absorption onset. By extrapolating this segment to its intersection with the energy axis [see inset of Fig. 9(b)], the energy gaps of the x-ray amorphous SnO_x films were estimated. Figure 9(c) shows these energy gaps as a function of substrate temperature.

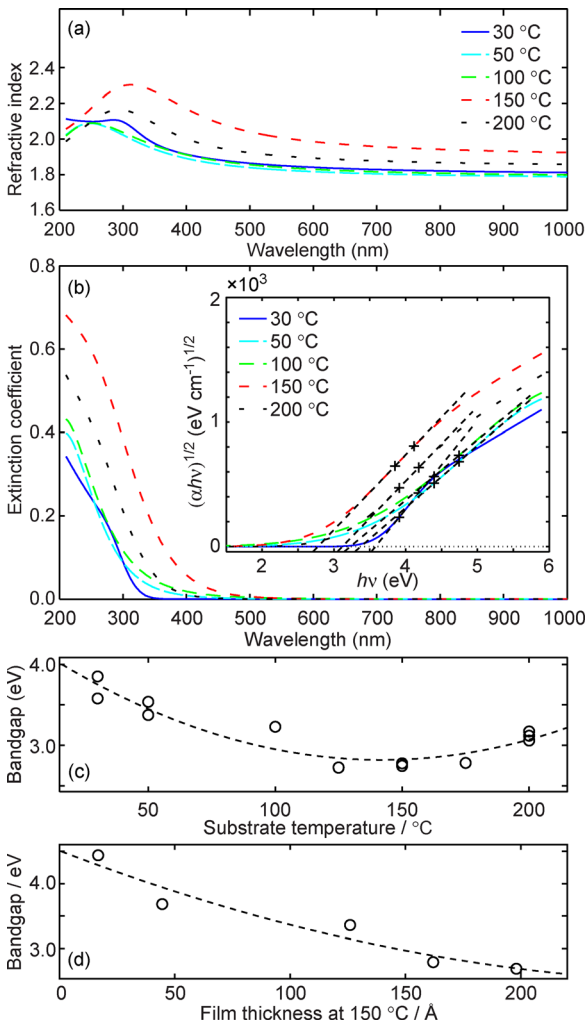

FIG. 9. (Color online) (a) SnO_x film refractive index and (b) extinction coefficient extracted from spectroscopic ellipsometry, as a function of the substrate temperature for films deposited using 200 ALD cycles. The inset in (b) illustrates plots of $(\alpha\, h\nu)^{1/2}$ with linear fits (dashed lines) to the approximately linear portion of the curve. Bandgaps are estimated from the intersection of the linear fits with $(\alpha\, h\nu)^{1/2} = 0$. (c) Estimated bandgaps as a function of temperature, after 200 cycles of ALD. (d) Bandgaps as a function of film thickness for varying number of ALD cycles and a substrate temperature fixed to 150 °C. The dashed lines in (c) and (d) represent quadratic fits to the data.

The bandgaps of Fig. 9(c) reveal a significant temperature dependence, with a minimum occurring around 150 °C. Because the number of ALD cycles was fixed in this experiment, the varying growth rates (Fig. 4) means that the film thickness were higher for the lower temperatures. To investigate if the observed bandgaps and other properties depend on the film thickness, additional experiments at fixed temperature (150 °C) and a varying number of ALD cycles were performed. The results, shown in Fig. 9(d), indicate a monotonic decrease of bandgap with thickness, from 4.4 eV for the thinnest (approximately 2 nm) film down to 2.7 eV for the thickest (20 nm) film. The film thickness dependence may therefore possibly explain the increasing trend at the highest temperatures of Fig. 9(c). Although the underlying mechanism for this thickness dependence is not yet known, we speculate that the films, rather than being purely amorphous, may form a fine-grained microstructure undetectable to XRD and with feature sizes related to the film thickness.[84] If the grains confine the wave functions of excited states, the bandgap will be affected by their size, with smaller grains exhibiting larger bandgaps. Since the exciton Bohr radius of SnO_2 quantum dots has been estimated to 2.7 nm,[26] it seems feasible that effects related to quantum confinement could be observed for the range of thicknesses covered here. Similar reasoning could be used to explain the increasing bandgap at lower temperatures, where growth conditions rather than film thickness would favor smaller grain sizes and therefore higher bandgap.[84] The minimum bandgap at 150 °C may then plausibly be the result of a maximum grain size, for the particular situation after 200 ALD cycles. Further characterization, for instance by transmission electron microscopy, would be needed to clarify this sensitive dependence of the optical properties on film thickness and substrate temperature in SnO_x thin films. In this context, it is also noteworthy that the growth rate increases by more than a factor 2 as the substrate temperature is reduced from 100 to 30 °C (Fig. 4). One may suspect that a lower mobility of surface species at low temperature would lead to a more porous film, and perhaps a concomitant higher growth rate. However, as the refractive indices are essentially the same over the whole spectrum in this temperature interval [Fig. 9(a)], film porosity is unlikely to account for increased growth rate, and an explanation based on the surface coverage of hydroxyl groups, outlined above, appears more plausible.

IV. SUMMARY AND CONCLUSIONS

By exploring in detail the use of water as a counter-reactant, this work expands on the application of TDMASn for the deposition of high quality tin oxide films in a low temperature range of 30–200 °C. Spectroscopic analyses show no appreciable change in elemental composition as a function of deposition temperature. Morphological and topographical analyses show that as-deposited SnO_x film is

relatively smooth, with only small crystalline features. XRD measurements before and after annealing in inert atmosphere show that the deposited films consist of x-ray amorphous SnO_2 which transform to rutile SnO_2 after annealing. The optical properties of the films display an interesting dependence on both deposition temperature and film thickness. Thin films grown at low temperature (30 °C) have relatively high bandgaps in excess of 4.0 eV, while thicker films grown at 150 °C have bandgaps below 3 eV. Thus, SnO_x films of high purity may to some extent be grown with tailored properties using this ALD process. This scheme for SnO_x ALD can allow for electrically and optically useful films, such as for transparent conductors and solar cell buffer layers, to be produced from earth abundant and inexpensive raw materials. The ability to grow this important metal oxide at near room temperature may further be favorable for biological applications and in industrial processes where reduced thermal demands are desired.

ACKNOWLEDGMENTS

The authors thank Han Zhou for AFM measurements. This work was supported by the Center for Nanostructuring for Efficient Energy Conversion, an Energy Frontier Research Center (EFRC) funded by the U.S. Department of Energy, Office of Basic Energy Sciences, Award No. DE-SC0001060. M.N.M. acknowledges the Bell Labs Graduate Fellowship Research Fellowship Program for graduate fellowship support. C.H. is grateful for financial support from the Marcus and Amalia Wallenberg Foundation.

[1]J. L. G. Fierro, *Metal Oxides: Chemistry and Applications* (CRC/Taylor & Francis, Boca Raton, FL, 2006).
[2]H. Ogawa, A. Abe, M. Nishikawa, and S. Hayakawa, J. Electrochem. Soc. **128**, 2020 (1981).
[3]K. Ishiguro, T. Sasaki, T. Arai, and I. Imai, J. Phys. Soc. Jpn. **13**, 296 (1958).
[4]M. Batzill and U. Diebold, Prog. Surf. Sci. **79**, 47 (2005).
[5]P. Cox, *The Surface Science of Metal Oxides* (Cambridge University Press, Cambridge, NY, 1994).
[6]J. Watson, Sens. Actuators **5**, 29 (1984).
[7]B. Panchapakesan, D. L. DeVoe, M. R. Widmaier, R. Cavicchi, and S. Semancik, Nanotechnology **12**, 336 (2001).
[8]C. J. Martinez, B. Hockey, C. B. Montgomery, and S. Semancik, Langmuir **21**, 7937 (2005).
[9]A. Kolmakov, Y. Zhang, G. Cheng, and M. Moskovits, Adv. Mater. **15**, 997 (2003).
[10]H. De Waal and F. Simons, Thin Solid Films **77**, 253 (1981).
[11]M. Vergohl, N. Malkomes, T. Matthee, G. Brauer, U. Richter, F. W. Nickol, and J. Bruch, Thin Solid Films **392**, 258 (2001).
[12]R. G. Gordon, J. Proscia, F. B. Ellis, Jr., and A. E. Delahoy, Sol. Energy Mater. **18**, 263 (1989).
[13]H. Klasens, Solid State Electron. **7**, 701 (1964).
[14]H. K. Liao, J. C. Chou, W. Y. Chung, T. P. Sun, and S. K. Hsiung, Sens. Actuators B **50**, 104 (1998).
[15]F. Chen and M. Liu, Chem. Commun. **1999**, 1829.
[16]P. Gao, Y. Ding, and Z. Wang, Nano Lett. **3**, 1315 (2003).
[17]A. Hagemeyer, Z. Hogan, M. Schlichter, B. Smaka, G. Streukens, H. Turner, A. Volpe, H. Weinberg, and K. Yaccato, Appl. Catal., A **317**, 139 (2007).
[18]S. Ferrere, A. Zaban, and B. A. Gregg, J. Phys. Chem. B **101**, 4490 (1997).
[19]J. S. Lee *et al.*, J. Cryst. Growth **254**, 443 (2003).
[20]R. Gordon, J. Non-Cryst. Solids **218**, 81 (1997).
[21]T. Minami, Thin Solid Films **516**, 5822 (2008).
[22]J. Proscia and R. G. Gordon, Thin Solid Films **214**, 175 (1992).
[23]R. B. H. Tahar, T. Ban, Y. Ohya, and Y. Takahashi, J. Appl. Phys. **83**, 2631 (1998).
[24]G. Sanon, R. Rup, and A. Mansingh, Thin Solid Films **190**, 287 (1989).
[25]J. Kane, H. Schweizer, and W. Kern, J. Electrochem. Soc. **122**, 1144 (1975).
[26]E. J. H. Lee, C. Ribeiro, T. R. Giraldi, E. Longo, E. R. Leite, and J. A. Varela, Appl. Phys. Lett. **84**, 1745 (2004).
[27]R. D. Tarey and T. A. Raju, Thin Solid Films **128**, 181 (1985).
[28]J. Sundqvist, J. Lu, M. Ottosson, and A. Hårsta, Thin Solid Films **514**, 63 (2006).
[29]S. H. Park, Y. C. Son, W. S. Willis, S. L. Suib, and K. E. Creasy, Chem. Mater. **10**, 2389 (1998).
[30]V. Brinzari, G. Korotcenkov, and V. Golovanov, Thin Solid Films **391**, 167 (2001).
[31]G. Sberveglieri, Sens. Actuators B **6**, 239 (1992).
[32]J. Heo, A. S. Hock, and R. G. Gordon, Chem. Mater. **22**, 4964 (2010).
[33]G. Choi, L. Satyanarayana, and J. Park, Appl. Surf. Sci. **252**, 7878 (2006).
[34]M. Utriainen, H. Lattu, H. Viirolä, L. Niinistö, R. Resch, and G. Friedbacher, Mikrochim. Acta **133**, 119 (2000).
[35]J. W. Elam, D. A. Baker, A. J. Hryn, A. B. F. Martinson, M. J. Pellin, and J. T. Hupp, J. Vac. Sci. Technol. A **26**, 244 (2008).
[36]X. Du, Y. Du, and S. George, J. Vac. Sci. Technol. A **23**, 581 (2005).
[37]C. Dücsö, N. Q. Khanh, Z. Horváth, I. Bársony, M. Utriainen, S. Lehto, M. Nieminen, and L. Niinistö, J. Electrochem. Soc. **143**, 683 (1996).
[38]J. Heo, S. B. Kim, and R. G. Gordon, J. Mater. Chem. **22**, 4599 (2012).
[39]D. H. Kim, J.-H. Kwon, M. Kim, and S.-H. Hong, J. Cryst. Growth **322**, 33 (2011).
[40]J. J. Robbins, R. T. Alexander, M. Bai, Y. J. Huang, T. L. Vincent, and C. A. Wolden, J. Vac. Sci. Technol. A **19**, 2762 (2001).
[41]J. Sundqvist, A. Tarre, A. Rosental, and A. Harsta, Chem. Vap. Deposition **9**, 21 (2003).
[42]H. Viirolä and L. Niinistö, Thin Solid Films **251**, 127 (1994).
[43]V. E. Drozd and V. B. Aleskovski, Appl. Surf. Sci. **82–83**, 591 (1994).
[44]C. Marichy, N. Donato, M.-G. Willinger, M. Latino, D. Karpinsky, S.-H. Yu, G. Neri, and N. Pinna, Adv. Funct. Mater. **21**, 658 (2011).
[45]S. M. George, Chem. Rev. **110**, 111 (2010).
[46]M. Leskelä and M. Ritala, Thin Solid Films **409**, 138 (2002).
[47]T. Aaltonen, M. Ritala, T. Sajavaara, J. Keinonen, and M. Leskela, Chem. Mater. **15**, 1924 (2003).
[48]R. L. Puurunen, J. Appl. Phys. **97**, 121301 (2005).
[49]M. Ritala and M. Leskelä, *Handbook of Thin Films*, edited by H. S. Nalva (Academic Press, San Diego, 2001), Vol. 1, pp. 103.
[50]H. Kim, Surf. Coat. Technol. **200**, 3104 (2006).
[51]H. Kim, J. Vac. Sci. Technol. B **21**, 2231 (2003).
[52]B. S. Lim, A. Rahtu, and R. G. Gordon, Nat. Mater. **2**, 749 (2003).
[53]T. Aaltonen, M. Ritala, V. Sammelselg, and M. Leskela, J. Electrochem. Soc. **151**, G489 (2004).
[54]D. B. Farmer and R. G. Gordon, Electrochem. Solid-State Lett. **8**, G89 (2005).
[55]X. Wang, S. M. Tabakman, and H. Dai, J. Am. Chem. Soc. **130**, 8152 (2008).
[56]M. M. Frank, G. D. Wilk, D. Starodub, T. Gustafsson, E. Garfunkel, Y. J. Chabal, J. Grazul, and D. A. Muller, Appl. Phys. Lett. **86**, 152904 (2005).
[57]M. Ritala, K. Kukli, A. Rahtu, P. I. Raisanen, M. Leskelä, T. Sajavaara, and J. Keinonen, Science **288**, 319 (2000).
[58]J. Y. Kim and S. M. George, J. Phys. Chem. C **114**, 17597 (2010).
[59]L. Reijnen, B. Meester, A. Goossens, and J. Schoonman, Chem. Vap. Deposition **9**, 15 (2003).
[60]P. Sinsermsuksakul, J. Heo, W. Noh, A. S. Hock, and R. G. Gordon, Adv. Energy Mater. **1**, 1116 (2011).
[61]E. B. Yousfi, B. Weinberger, F. Donsanti, P. Cowache, and D. Lincot, Thin Solid Films **387**, 29 (2001).
[62]Y. Hua, W. P. King, and C. L. Henderson, Microelectron. Eng. **85**, 934 (2008).
[63]X. Jiang and S. F. Bent, J. Electrochem. Soc. **154**, D648 (2007).
[64]X. Jiang and S. F. Bent, J. Phys. Chem. C **113**, 17613 (2009).
[65]H.-B.-R. Lee, K. Jaemin, K. Hyungjun, K. Woo-Hee, L. Jeong Won, and H. Inchan, J. Korean Phys. Soc. **56**, 104 (2010).
[66]W. Lee and F. B. Prinz, J. Electrochem. Soc. **156**, G125 (2009).
[67]M. N. Mullings, H.-B.-R. Lee, N. Marchack, X. Jiang, Z. Chen, Y. Gorlin, K.-P. Lin, and S. F. Bent, J. Electrochem. Soc. **157**, D600 (2010).

[68]R. H. A. Ras, E. Sahramo, J. Malm, J. Raula, and M. Karppinen, J. Am. Chem. Soc. **130**, 11252 (2008).
[69]A. Sinha, D. W. Hess, and C. L. Henderson, Proc. SPIE **6519**, 65191J (2007).
[70]D. B. Farmer and R. G. Gordon, Nano Lett. **6**, 699 (2006).
[71]C. F. Herrmann, F. H. Fabreguette, D. S. Finch, R. Geiss, and S. M. George, Appl. Phys. Lett. **87**, 123110 (2005).
[72]W.-H. Kim, S.-J. Park, J.-Y. Son, and H. Kim, Nanotechnology **19**, 045302 (2008).
[73]J. S. King, D. Heineman, E. Graugnard, and C. J. Summers, Appl. Surf. Sci. **244**, 511 (2005).
[74]I. M. Povey, M. Bardosova, F. Chalvet, M. E. Pemble, and H. M. Yates, Surf. Coat. Technol. **201**, 9345 (2007).
[75]A. Yamada, B. S. Sang, and M. Konagai, Appl. Surf. Sci. **112**, 216 (1997).
[76]B. S. Sang and M. Konagai, Jpn. J. Appl. Phys., Part 2 **35**, L602 (1996).
[77]C. A. Hoel, T. O. Mason, J. F. Gaillard, and K. R. Poeppelmeier, Chem. Mater. **22**, 3569 (2010).
[78]R. Methaapanon, S. M. Geyer, C. Hägglund, P. A. Pianetta, and S. F. Bent, Rev. Sci. Instrum. **84**, 015104 (2013).
[79]See supplementary material at http://dx.doi.org/10.1116/1.4812717 for carbon contamination determined by X-ray photoelectron spectroscopy.
[80]C. Herzinger and B. Johs, *Guide to Using WVASE32* (J.A. Woollam Company, Lincoln, NE, 1996).
[81]D. Davazoglou, Thin Solid Films **302**, 204 (1997).
[82]J. Melsheimer and D. Ziegler, Thin Solid Films **129**, 35 (1985).
[83]J. Tauc, R. Grigorov, and A. Vancu, Phys. Status Solidi **15**, 627 (1966).
[84]M. Ohring, *Materials Science of Thin Films* (Stevens Institute of Technology, Hoboken, NJ, 2002).